Trilayer Tunnel Selectors for Memristor Memory Cells

Byung Joon Choi, Jiaming Zhang, Kate Norris, Gary Gibson, Kyung Min Kim, Warren Jackson, Min-Xian Max Zhang, Zhiyong Li, J. Joshua Yang, and R. Stanley Williams**

In order to achieve extremely high densities on a nonvolatile memory (NVM) die (>100 Gbit cm^{-2}), resistance switches, or memristors, need to be connected together in large arrays to amortize the silicon circuitry utilized to address, write, and read individual bits.[1–3] Although individual devices with sub-10 nm feature sizes and promising switching characteristics have been demonstrated,[3,4] the leakage current through unselected devices during WRITE and/or READ operations limits the size of the array and thus the bit density of a NVM die. Thus, unless the memristor itself has a large intrinsic nonlinear current–voltage (*i*–*v*) response, some type of selector is required in series with the switch in a memory cell to form the so-called 1S1R configuration. For unipolar devices, the selector can be a diode, but for bipolar memristors, the selector needs to have a large and roughly symmetric *i*–*v* nonlinearity in order to block current flow in either direction at low voltage magnitudes while allowing a much larger (e.g., >100×) current at higher voltages. Therefore, two-terminal selectors with a scalability comparable to that of memristors are essential to realize the large array sizes needed to be competitive with the bit densities of alternate NVM technologies.[2,3,5–13] Accordingly, a significant effort has recently introduced a variety of new selectors, including an Ovonic threshold switch,[11,14] a mixed ionic–electronic conductor,[9] an insulator–metal-transition[5,15,16] selector, tunneling devices,[12,17–20] and others.[6,13]

Among these selectors, tunnel barriers are especially promising because of their high durability and intrinsic speed. The endurance of a selector needs to be significantly greater than that of its companion memristor because the selector should be turned ON not only for every memristor programming event but also for every READ operation. Reproducibility of their *i*–*v* characteristics is required to enable consistent switching from cycle to cycle and minimize variability in the READ signal. In principle, tunnel selectors possess other advantages, such as well-understood physical mechanisms and accurate mathematical modeling, low (possibly no) temperature dependence of resistance and low energy consumption (no Joule heating required).

Despite the advantages of tunneling, the *i*–*v* nonlinearity of a single-layer barrier of any commonly available material is usually insufficient for selector applications. Likharev proposed and demonstrated theoretically that a graded or crested tunnel barrier could be engineered to enhance the nonlinearity.[21] Simulations have been used to show that a simple trilayer structure consisting of a dielectric with a smaller electron affinity (usually larger bandgap) sandwiched between two other dielectric layers with a larger electron affinity (usually smaller bandgap) can yield a very large nonlinearity.[21,22] A high nonlinearity was observed experimentally in a $TaO_x/TiO_2/TaO_x$ trilayer structure and attributed to the crested barrier effect.[12] However, the electron affinity of the middle layer (TiO_2, ≈4.1 eV)[12,23,24] should be larger than that of the outer layers (Ta_2O_5, ≈3.2 eV)[12,25] in this case, which was opposite to the proposed design of a crested barrier.[21,22] Defects created by the diffusion of Ta into TiO_2 were assumed to somehow lead to the formation of a crested barrier, but this proposal requires further clarification.[12] Recently, encouraging *i*–*v* nonlinearity and current density were obtained from multilayered selector devices inspired by the crested barrier concept, such as *a*-Si/SiN_x/*a*-Si and $Ta_2O_5/TaO_x/TiO_2$ trilayers.[18,20,26] Therefore, it is of great interest to carefully examine the crested barrier concept by understanding the physics and chemistry of the multilayer and its components, as well as the complicated interfaces and barrier structures.

We have observed a significant increase in *i*–*v* nonlinearities for a trilayer tunnel barrier (TLTB) compared to a single-layer dielectric, and demonstrate here the feasibility of integrating a TLTB selector with a typical TaO_x memristor, which normally has a fairly linear *i*–*v* characteristic, to obtain highly nonlinear integrated cells. **Figure 1**a shows the quasistatic *i*–*v* plots of junction devices with different barrier layers: a 27 nm stoichiometric TaN layer, single TaN_{1+x} semiconducting layers (5 and 10 nm), and a TLTB stack of TaN_{1+x} (3 nm)/Ta_2O_5 (2.5 nm)/TaN_{1+x} (3 nm). Metallic nitride materials, such as TaN, TiN, and WN, are widely used as contact electrodes in the complementary metal–oxide semiconductor (CMOS) fab. Ta_2O_5 is one of the leading memristive materials and also available in the CMOS fab. TaN_{1+x} exhibits a transition from metal to insulator with increasing nitrogen content.[27] The insulator phase has a smaller bandgap (≈2 eV) than Ta_2O_5 and a larger electron affinity, which together with its chemical compatibility with the TaN electrode makes TaN_{1+x} a natural choice for the outer layers of a crested barrier consisting of Ta_2O_5 (larger bandgap and smaller electron affinity) as the middle layer. In order to maintain the chemical integrity of the electrode/barrier interfaces so that the intrinsic properties of the barrier layers could be studied, the inert metal Pt was adopted for both top

Prof. B. J. Choi,[+] Dr. J. Zhang, Dr. K. Norris, Dr. G. Gibson, Dr. K. M. Kim, Dr. W. Jackson, Dr. M.-X. M. Zhang, Dr. Z. Li, Prof. J. J. Yang,[++] Dr. R. S. Williams
Hewlett Packard Laboratories
Palo Alto, CA 94304, USA
E-mail: jjyang@umass.edu; stan.williams@hpe.com

[+]Present Address: The Department of Materials Science and Engineering, Seoul National University of Science and Technology, Seoul, 139-743, South Korea
[++]Present Address: The Department of Electrical and Computer Engineering, University of Massachusetts, Amherst, MA 01003, USA

DOI: 10.1002/adma.201503604

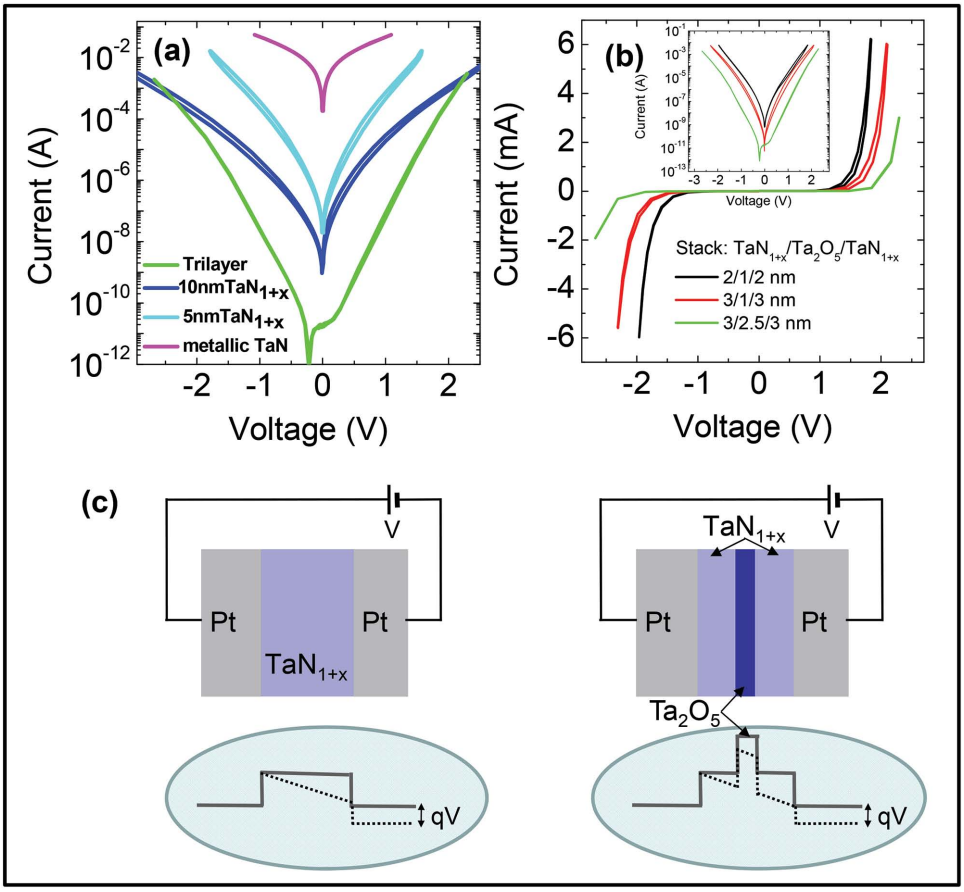

Figure 1. Single-layer and trilayer tunnel barriers. a) *i–v* characteristics of two different single TaN_{1+x} layer (5 and 10 nm) barriers compared to a trilayer (3 nm TaN_{1+x}/2.5 nm Ta_2O_5/3 nm TaN_{1+x}) barrier. b) Three trilayer devices with different thickness of each layer: 2/1/2, 3/1/3, and 3/2.5/3 nm (inset) in semilog plot. c) Schematic diagrams of the single and trilayer barrier structures and band diagrams.

and bottom electrodes, which were patterned by shadow masks (10 μm × 10 μm in a cross-point configuration) instead of photolithography and etching to further minimize possible interlayer chemical contamination. The TLTB device exhibited a highly nonlinear *i–v* characteristic, i.e., fairly insulating under low bias (e.g., ≈270 nA at +1 V) and highly conductive at high bias (e.g., ≈3 mA at +2 V). We define the nonlinearity k of an *i–v* curve as $k = i(v_{op})/i(v_{op}/2)$ for the half-voltage operation scheme, in which half of the operation voltage v_{op} (applied on the selected cell for reading or writing) drops across all the cells that share a column or row in a crossbar with the selected cell. The k value is exactly 2 for a linear *i–v* characteristic (e.g., the stoichiometric and metallic TaN in Figure 1a) and is higher for nonlinear *i–v* curves (e.g., the semiconducting layers in Figure 1a). According to this definition, the TLTB device exhibits a k value of 11,000 at V_{op} = +2 V, while single layers of TaN_{1+x} or Ta_2O_5 yield k values of only 50 or below at V_{op} = +2 V. A higher "operating" voltage on the TLTB selector usually leads to an even larger k value, but this voltage should match the operating voltages of the companion memristor and is constrained by the total voltage available from the driving circuitry for a crossbar.

The thickness dependence of the constituent layers of a TLTB device was examined. The *i–v* curves from three different samples are shown in Figure 1b. The samples are identified with the following notation: TaN_{1+x} (*a* nm)/Ta_2O_5 (*b* nm)/TaN_{1+x} (*c* nm), where *a*/*b*/*c* = 2/1/2, 3/1/3, or 3/2.5/3. The resistance and nonlinearity of the TLTB selector are sensitive to the thickness values of both the TaN_{1+x} and Ta_2O_5 layers. As shown in Figure 1a, doubling the single-layer TaN_{1+x} film thickness from 5 to 10 nm only moderately increased the resistance, suggesting that tunneling through the barrier was not the dominant electron transport mechanism in TaN_{1+x}. Moreover, the *i–v* nonlinearities of both the 5 and 10 nm layers remain low (<50) and insensitive to the barrier layer thickness. In contrast (Figure 1b), the k value of the TLTB devices increased dramatically to 580 (V_{op} = +1.9 V) in the 2/1/2 device and 1650 (V_{op} = +2 V) in the 3/1/3 device by inserting a 1 nm layer of Ta_2O_5 into the TaN_{1+x} films. In the TLTB devices, a greater TaN_{1+x} thickness increased not only the device resistance but also the nonlinearity. In addition, the k value was increased almost another order of magnitude to 11 000 by increasing the thickness of theTa_2O_5 layer in the 3/2.5/3 device. The band diagrams of the single barrier and TLTB devices are illustrated schematically in Figure 1c, and will be discussed in more detail below.

A TLTB selector was electrically connected to a discrete TaO_x memristor microdevice to evaluate the behavior of a combined 1S1R memory cell, as illustrated in **Figure 2**a. Compared with the integrated cell to be shown later, this configuration allowed

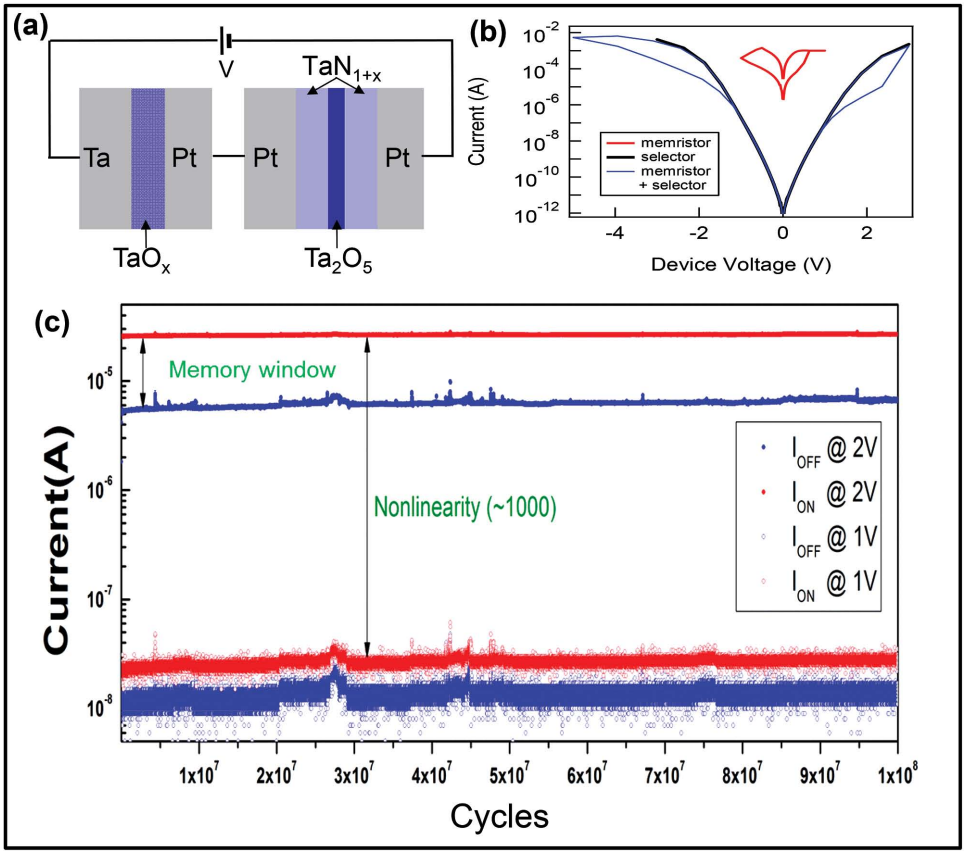

Figure 2. A 1S1R cell built by externally wiring a trilayer selector and a discrete TaO_x memristor. a) The circuit diagram of the memristor (left) connected with a trilayer selector (right). b) *i–v* curves of the individual elements (red and black) and the combined 1S1R cell (blue). c) Open loop electrical pulse switching of the combined 1S1R device up to 100 million cycles.

measurement of each component of the 1S1R cell separately to characterize their isolated behavior and then understand how they interact when connected in series. Figure 2b shows the measured *i–v* curves of the memristor, selector, and the 1S1R cell. The selector used for this experiment had a *k* value of ≈1300 at V_{read} = +2 V (black curve), which was selected for the demonstration because it provided voltage and current levels that best matched (among our existing TLTB selectors) the switching voltage and current of the TaO_x memristor. The TaO_x device displayed a linear *i–v* in the ON state. As can be seen from the *i–v* curves of the combined cell (blue curve), the selector limited the device current flow within the low bias voltage range (<1 V) while at high bias (>1 V) the selector was so conductive that the OFF state of the memristor limited the current (if the memristor was in its OFF state). The 1S1R cell switched ON at ≈+2.3 V. For RESET, a relatively high negative bias of ≈–5 V was needed to switch the 1S1R cell, because most of the applied voltage dropped across the selector and the wire until the memristor is switched nearly in its OFF state.

The switching characteristics of the cell were examined by programming and reading open loop with sequential SET, READ, RESET, and READ electrical pulses for 100 million cycles, as shown in Figure 2. Voltage pulses of +3.6 and –7 V were used for SET and RESET, respectively. Pulses of +2 and +1 V were consecutively applied for READ operations. All of the pulse widths were 2 µs, which was the shortest pulse duration in the purpose-built measurement system. The noise and other variability in the ON and OFF currents were much smaller than the difference between the two currents, making reading of the state very reliable. Because of the large cell *k* value of ≈1000, the leakage current levels for the ON and OFF states were both very low and barely distinguishable at half the READ voltage (1 V), showing that, in principle, such a system could support a large array of cells. In addition to providing nonlinearity for the cell, the selector acted as an internal regulator to dynamically adjust the electrical bias on the memristor and prevent runaway conductance changes during programming, which may have significantly contributed to the low cycle to cycle variability observed in Figure 2c. Prevention of capacitive charging currents and thermal disturbances from the circuits and neighboring memristors could be an advantage for this tunnel-based selector in a large array.[7,28,29]

To further understand the TLTB devices, we performed detailed physical and electrical characterization of the individual layers and multilayered structures. The TaN_{1+x} films were grown by atomic layer deposition (ALD) using an N-containing Ta metal organic precursor and an N_2:H_2 gas mixture (see the Experimental Section). As shown in Figure S1 (Supporting Information), results from X-ray diffraction and transmission electron microscope measurements revealed that the

hypostoichiometric TaN_{1+x} film was amorphous. In contrast, stoichiometric TaN films grown by ALD using the same Ta precursor but NH_3 gas (see the Experimental Section) were crystalline. Although the detailed chemical reactions of Ta precursor molecules with NH_3 (75% of H_2) plasma or mixed N_2:H_2 (2% of H_2) plasma are not known, plasma-activated hydrogen radicals have been reported to serve as an efficient reducing agent for the metal organic precursors.[30,31] The Ta precursors in these experiments contained amine groups, which can either form a stoichiometric TaN film after being reduced by abundant hydrogen radicals (e.g., in NH_3 plasma) or form a hypostoichiometric TaN_{1+x} when hydrogen radicals are more scarce (e.g., in the N_2: 2% H_2 plasma).[30–33] X-ray photoelectron spectroscopy measurements on the ALD films indicated that the TaN film using NH_3 plasma had a higher carbon impurity, which may also contribute to the conductivity of this nitride film by forming some Ta carbide inclusion in it. It was reported that Ta carbide has a much lower resistivity (≈20 μΩ cm) compared to that of TaN (≈250 μΩ cm) or Ta_2N. Decomposition of Ta precursors with a high plasma power may facilitate the formation of Ta–C rather than Ta–N compounds.[34] The indirect optical bandgap of a TaN_{1+x} film was determined by UV–vis absorption measurements to be about 2 eV (Figure S2, Supporting Information), close to reported values for Ta_3N_5 films.[32,35] The bandgap of the ALD Ta_2O_5 film was determined to be about 4.1 eV, much higher than that of the TaN_{1+x} films. The *i*–*v* curves for devices made using a single-layer barrier composed of the ALD Ta nitride films revealed essentially linear behavior consistent with stoichiometric TaN whereas devices incorporating the TaN_{1+x} films exhibited a nonlinear semiconducting behavior that is similar to that observed from a sputter-grown Ta_3N_5 barrier (Figure S3, Supporting Information). The impact of N content and crystallinity of the TaN_{1+x} film was also investigated. A higher N content and crystallinity enhanced the nonlinearity of TaN_{1+x} film (Figure S3, Supporting Information).

Temperature-dependent *i*–*v* curves provide more information on the electron transport mechanisms of the single barrier and TLTB elements, as shown in **Figure 3**. Interestingly, the element with the thicker barrier (7 nm TLTB) showed a weaker temperature dependence than that of the element with the thinner barrier (single 5 nm TaN_{1+x} layer). As shown in Figure 3c, the conduction data for the Pt/5 nm TaN_{1+x}/Pt device are consistent with the Schottky emission model, yielding a Schottky barrier height of about 0.6 eV from the *y*-intercept of the extrapolated data and a high-frequency dielectric constant of about 3.4 from the slope of the curve measured at room temperature (300 K). Here, the net current density (J^*) was determined by factoring out the backward current under the applied potential, $\frac{J}{1-\exp\left(-\frac{qV}{k_bT}\right)}$, and a correction factor (λ = 0.5) for the Richardson constant (A_R) was used in determining the Schottky barrier height from the *y*-intercept of Figure 3c.[36] The low barrier height indicates possible Fermi level pinning at the interface. The dielectric constant was almost identical to the value determined using single-wave ellipsometry of a similarly deposited film (using the relation $\varepsilon_i = n^2$).[37] A similar result was obtained from the estimation of the zero-field Schottky barrier height using the plot of $\ln(J/T^2)$ as a function of $1000/T$ at the low field region (40–640 kV cm^{-1}), as noted in Figure S4 (Supporting Information).[38] The addition of a thin Ta_2O_5 layer with its larger bandgap should make Schottky emission over the barrier negligible at the temperatures used to test the TLTB device. As anticipated, the transport mechanism in the TLTB device more resembled tunneling, as indicated by the significantly weaker temperature dependence of the current. When the applied electric field was sufficiently high (>1.4 MV cm^{-1}), the dependence of current on field mimicked that of Fowler–Nordheim tunneling, as shown in Figure 3d. The effective equivalent single-layer barrier height, $\varnothing_b$, under high electric field was ≈2.2 eV, as determined from the relation: $q\varnothing_b = \left(-\frac{3eh}{8\pi\sqrt{2m^*}}K\right)^{2/3}$ where q is the elementary charge, h is the Plank constant, K is the slope of the data plot, and m^* is the effective electron mass (fixed to 0.3 m_0).[39,40] The higher nonlinearity provided by the TLTB device was not surprising given its expected "crested" nature. The electron affinity of Ta_3N_5 is ≈4 eV,[33] which is larger than that generally reported for the middle Ta_2O_5 barrier layer (≈3.2 eV).[12,25,41] Thus, we expected the tunneling barrier provided by the TLTB devices to decrease not only in width but also in height, as predicted by Likharev[21] at high applied fields, leading to the much higher nonlinearity observed in the TLTB selectors. Based on the conduction model and experimental results, nonlinearity and current density values are represented as a function of film thickness in single TaN_{1+x} and TLTB devices in Figure 3e.

A cell combining both TLTB and TaO_x memristor layers was built and analyzed to demonstrate the feasibility of integration, as shown by the cross-section STEM (scanning transmission electron microscope) micrograph and EELS (electron energy loss spectroscopy) line profiles for some key elements in **Figure 4**a. Repeatable switching hysteresis loops obtained from the integrated cell are presented in Figure 4b, showing nonlinear *i*–*v* characteristics for the ON state that contrast with the linear *i*–*v* relation for a "bare" TaO_x memristor. The switching voltages in this integrated cell were significantly reduced compared with the externally wired 1S1R cell in Figure 2a because of the higher resistance of the ON state of the memristor in the integrated cell. The reduced nonlinearity (≈100) in this integrated cell is attributed to the lower effective barrier height owing to the lower work function of the electrode material (W_M), in this case, Ta ($4 < W_{Ta} < 4.8$ eV) or TiN ($4.2 < W_{Ta} < 4.5$ eV) compared to Pt ($W_{Pt} \approx 5.5$ eV). In addition, the inert Pt electrode can alleviate the formation of an interfacial layer during an ALD or sputtering process. TiN or Ta electrodes may further reduce the effective barrier height, due to the formation of an interfacial layer, which results in an increased charge injection and diminished nonlinearity as shown in Figure S3 (Supporting Information).

Scalability and device variability are concerns because of the increased number of processes and film stacks with various thicknesses and compositions. The nonlinearity and variability (device to device) of the TLTB selector did not deteriorate when scaled down to 40 nm diameter (Figures S5 and S6, Supporting Information). However, the current level at a given voltage was also largely scaled down, which has to be solved by further optimizing materials and processes.

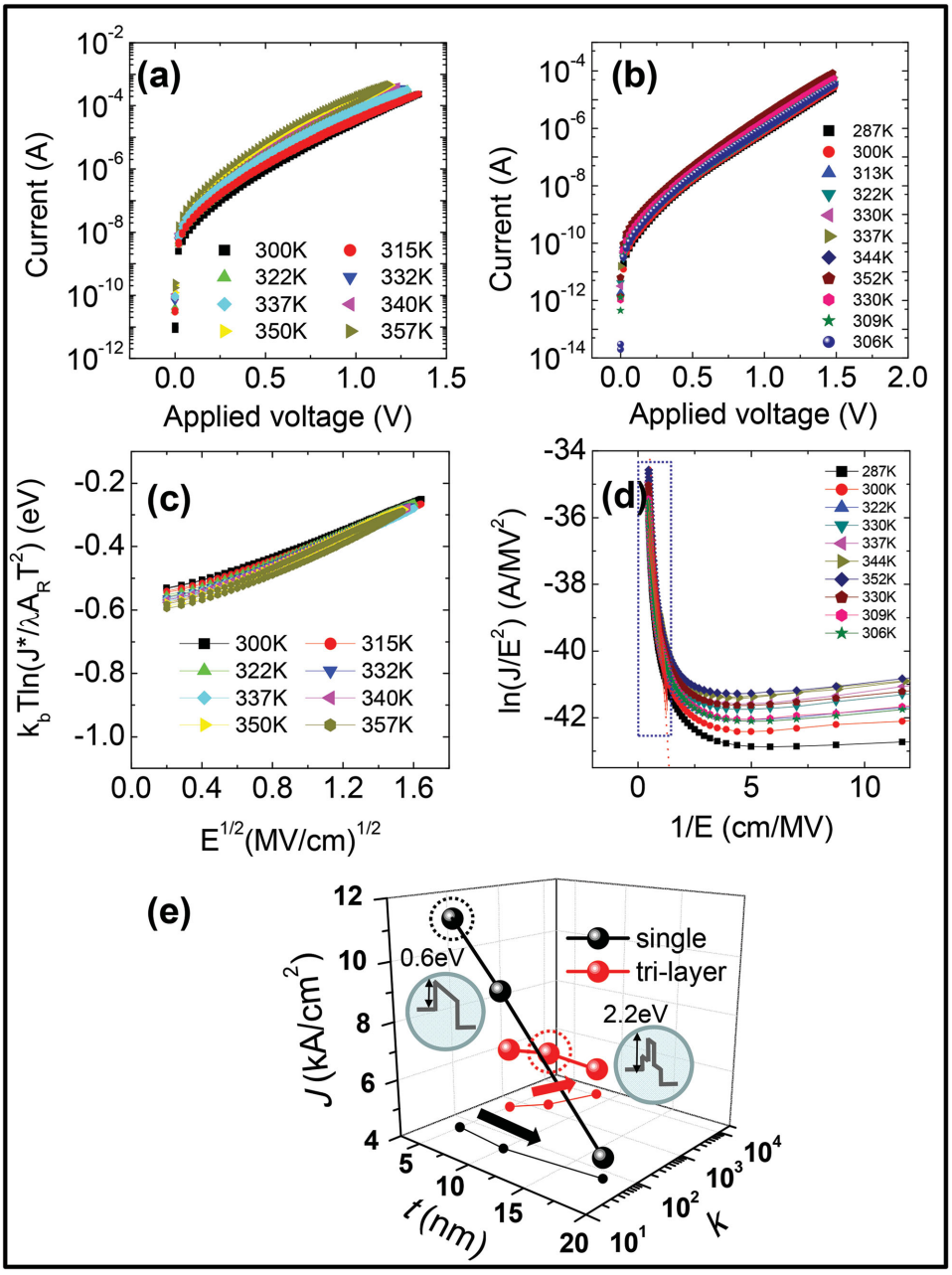

Figure 3. Electron transport of the single-layer and trilayer barriers at various temperatures. Measured data from a) the 5 nm TaN_{1+x} single layer exhibit larger temperature dependence than that of b) a 3 nm TaN_{1+x}/1 nm Ta_2O_5/3 nm TaN_{1+x} trilayer. c) The same data plotted in different formats show that the single-layer barrier exhibits Schottky-like thermionic emission fitted with a barrier height ≈0.6 eV, while d) the trilayer barrier resembles Fowler–Nordheim tunneling under sufficiently high field (>1.4 MV cm^{-1} in the dotted box). e) Nonlinearity and current density as a function of film thickness.

In summary, only moderate *i–v* nonlinearities were obtained with single-layer tunnel barriers, while a significant increases in the nonlinearities were demonstrated by all ALD grown TaN_{1+x} / Ta_2O_5 /TaN_{1+x} TLTBs. With the TLTB, both the barrier height and effective width were reduced simultaneously under high voltage bias, yielding a significantly larger nonlinearity exceeding 10 000 without any forming or conditioning process. High endurance (>10^8), low variability, and low temperature dependence were also observed with TLTBs. The feasibility of using this selector with a typical memristor has been demonstrated by externally wiring the selector to a discrete memristor as well as by physically integrating them into a multilayered 1S1R cell.

Experimental Section

Device Fabrication: Devices were fabricated on thermally grown 200 nm thick SiO_2 on a Si substrate. Various thin films were deposited by remote plasma enhanced ALD using (*t*-butylimido)tris(dimethylamido)tantalum (TBTMET, SAFC Hitech) as a metal organic precursor. Mixed N_2:H_2 (40:1 SCCM) gas or NH_3 (50 SCCM) was adopted as a reactant gas

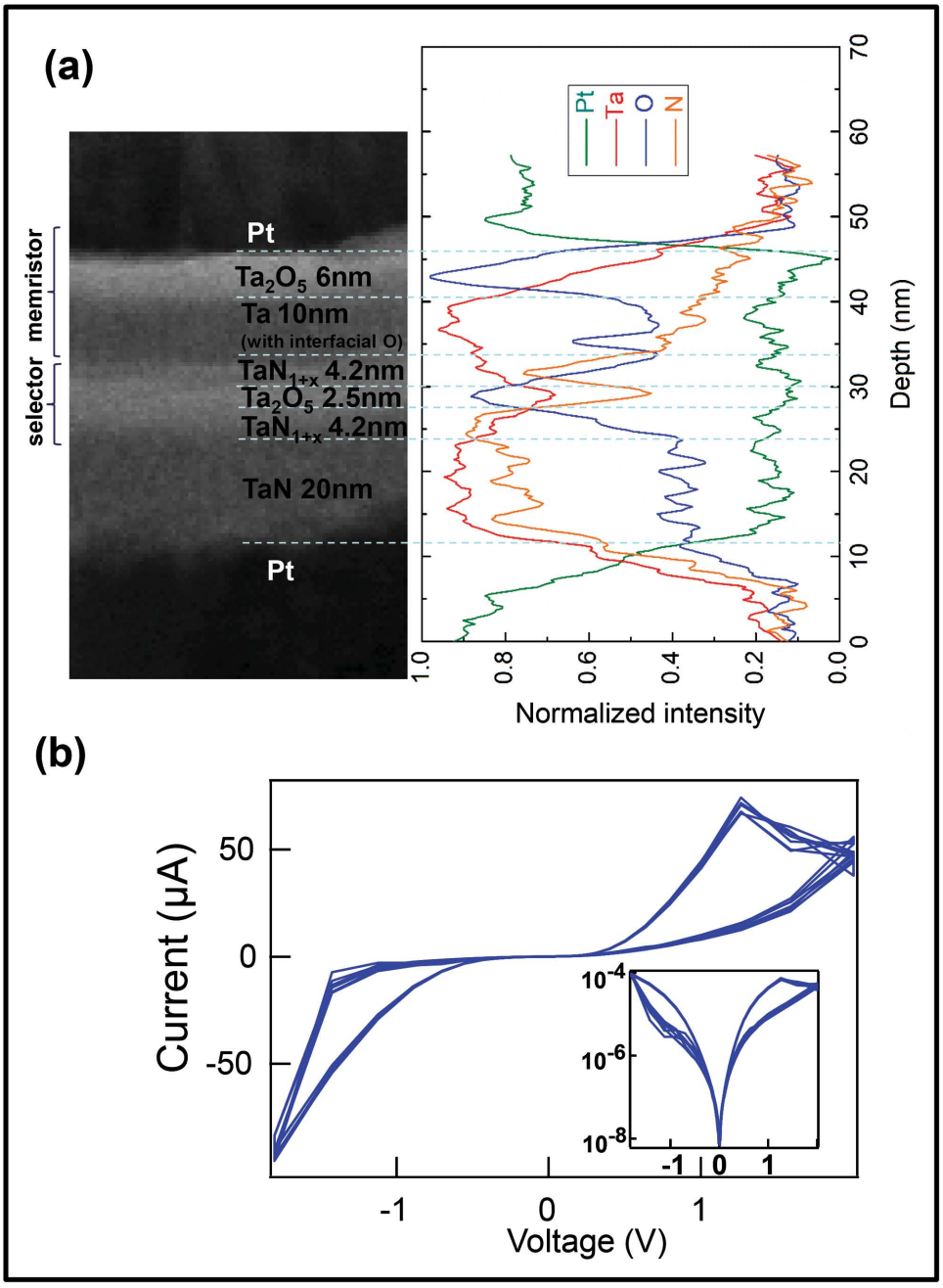

Figure 4. Integrated 1S1R cell. a) STEM bright field image and EELS line profiles of the cross-section of the integrated cell. b) The typical quasi-DC switching *i–v* loops of the integrated cell. The inset to panel (b) has the same data in a semilog plot.

on purpose to change the physical properties of thin film devices. O_2 (50 SCCM) plasma ALD process was used for creating the Ta_2O_5 barrier layer. ALD cycle and conditions for TaN_x and Ta_2O_5 films are represented in Table S1 of the Supporting Information. Growth temperature was varied from 300 to 400 °C. For the cross-point device, a 20 nm thick electron-beam evaporated Pt ribbon was used as the bottom electrode, for which a very thin (≈1 nm) Ta film was used as the adhesion layer. Blanket thin film tunnel barriers were grown by ALD on top of the bottom electrode ribbon, and then a Pt top electrode was deposited by electron-beam evaporation through a shadow mask forming cross-point junction device.

Characterization: The four-terminal *i–v* characteristics of the devices were measured using a semiconductor parameter analyzer (HP-4156), which can extract the actual voltage drop on the device from the total applied voltage. A quasi-DC voltage sweep was applied to the top electrode with the bottom contact grounded at ambient temperature in all the electrical measurements. The crystallinity of the films was analyzed using an X-ray diffractometer. The bandgap of the TaN_x films was determined optically by UV–vis absorption spectroscopy. The atomic concentrations and contaminants in the TaN_x thin film were measured by Rutherford backscattering spectroscopy and X-ray photoelectron microscopy, which revealed the mixed N_2:H_2 reactant gas may lead to slightly more N concentration in the film, while the NH_3 reactant gas results in a few percent C impurity in the nitride film. The aberration-corrected STEM/EELS analysis was performed using a

FEI Titan transmission electron microscopy at an accelerating voltage of 300 KV.

Supporting Information

Supporting Information is available from the Wiley Online Library or from the author.

Acknowledgments

B.J.C. was supported by Basic Science Research Program through the National Research Foundation of Korea (NRF) funded by the Ministry of Education (2014R1A1A2054597).

Received: July 24, 2015
Revised: September 18, 2015
Published online: November 19, 2015

[1] R. Waser, R. Dittmann, G. Staikov, K. Szot, *Adv. Mater.* **2009**, *21*, 2632.
[2] M.-J. Lee, C. B. Lee, D. Lee, S. R. Lee, M. Chang, J. H. Hur, Y. Kim, C. Kim, D. H. Seo, S. Seo, U. Chung, I. Yoo, K. Kim, *Nat. Mater.* **2011**, *10*, 625.
[3] B. Govoreanu, G. S. Kar, Y. Chen, V. Paraschiv, S. Kubicek, A. Fantini, I. P. Radu, L. Goux, S. Clima, R. Degraeve, N. Jossart, O. Richard, T. Vandeweyer, K. Seo, P. Hendrickx, G. Pourtois, H. Bender, L. Altimime, D. J. Wouters, J. A. Kittl, M. Jurczak, B. Leuven, K. U. Leuven, *IEDM Technical Digest*, IEEE, San Francisco, California, USA **2011**, p.729.
[4] S. Pi, M. Ghadiri-Sadrabadi, J. C. Bardin, Q. Xia, *Nat. Commun.* **2015**, *6*, 7519.
[5] M.-J. Lee, Y. Park, D.-S. Suh, E.-H. Lee, S. Seo, D.-C. Kim, R. Jung, B.-S. Kang, S.-E. Ahn, C. B. Lee, D. H. Seo, Y.-K. Cha, I.-K. Yoo, J.-S. Kim, B. H. Park, *Adv. Mater.* **2007**, *19*, 3919.
[6] E. Linn, R. Rosezin, C. Kügeler, R. Waser, *Nat. Mater.* **2010**, *9*, 403.
[7] G. H. Kim, J. H. Lee, Y. Ahn, W. Jeon, S. J. Song, J. Y. Seok, J. H. Yoon, K. J. Yoon, T. J. Park, C. S. Hwang, *Adv. Funct. Mater.* **2012**, *23*, 1440.
[8] J. J. Yang, M.-X. Zhang, M. D. Pickett, F. Miao, J. Paul Strachan, W.-D. Li, W. Yi, D. A. A. Ohlberg, B. J. Choi, W. Wu, J. H. Nickel, G. Medeiros-Ribeiro, R. Stanley Williams, *Appl. Phys. Lett.* **2012**, *100*, 113501.
[9] G. W. Burr, K. Virwani, R. S. Shenoy, A. Padilla, M. Brightsky, E. A. Joseph, M. Lofaro, A. J. Kellock, R. S. King, K. Nguyen, A. N. Bowers, M. Jurich, C. T. Rettner, B. Jackson, D. S. Bethune, R. M. Shelby, T. Topuria, N. Arellano, P. M. Rice, B. N. Kurdi, K. Gopalakrishnan, *VLSI*, IEEE, Honolulu, Hawaii, USA **2012**, p.41.
[10] H. D. Lee, S. G. Kim, K. Cho, H. Hwang, H. Choi, J. Lee, S. H. Lee, H. J. Lee, J. Suh, S. Chung, Y. S. Kim, K. S. Kim, W. S. Nam, J. T. Cheong, J. T. Kim, S. Chae, E. Hwang, S. N. Park, Y. S. Sohn, C. G. Lee, H. S. Shin, K. J. Lee, K. Hong, H. G. Jeong, K. M. Rho, Y. K. Kim, J. Nickel, J. J. Yang, H. S. Cho, F. Perner, R. S. Williams, J. H. Lee, S. K. Park, *VLSI*, 151, IEEE, Honolulu, Hawaii, USA **2012**, p.151.
[11] M.-J. Lee, D. Lee, H. Kim, H.-S. Choi, J.-B. Park, H. G. Kim, Y.-K. Cha, U.-I. Chung, I.-K. Yoo, K. Kim, *IEDM Technical Digest*, IEEE, San Francisco, California, USA **2012**, p.33
[12] W. Lee, J. Park, S. Kim, J. Woo, J. Shin, G. Choi, S. Park, D. Lee, E. Cha, B. H. Lee, H. Hwang, *ACS Nano* **2012**, *6*, 8166.
[13] S. Kim, D.-I. Moon, W. Lu, D. H. Kim, D. M. Kim, Y.-K. Choi, S.-J. Choi, *Appl. Phys. Lett.* **2013**, *103*, 033505.
[14] S. Kim, Y.-B. Kim, K. M. Kim, S.-J. Kim, S. R. Lee, M. Chang, I.-K. Y. M.-J. Lee, D. Lee, C. J. Kim, U.-I. Chung, *VLSI* **2013**, p. 240, IEEE, Kyoto, Japan.
[15] M. D. Pickett, J. Borghetti, J. J. Yang, G. Medeiros-Ribeiro, R. S. Williams, *Adv. Mater.* **2011**, *23*, 1730.
[16] S. Kim, X. Liu, J. Park, S. Jung, W. Lee, J. Woo, J. Shin, G. Choi, C. Cho, S. Park, D. Lee, E. Cha, B.-H. Lee, H. D. Lee, S. G. Kim, S. Chung, H. Hwang, *VLSI*. IEEE, Honolulu, Hawaii, USA **2012**, p.155.
[17] A. Kawahara, R. Azuma, Y. Ikeda, K. Kawai, Y. Katoh, Y. Hayakawa, K. Tsuji, S. Yoneda, A. Himeno, K. Shimakawa, T. Takagi, T. Mikawa, *IEEE J. Solid-State Circiuits* **2013**, *48*, 173.
[18] V. Govoreanu, B. Zhang, L. Crotti, D. Fan, Y.-S. Paraschiv, M. Hody, H. Witters, T. Meersschaut, J. Clima, S. Adelmann, C. Jurczak, *IEEE Inter. Mem. Work.* IEEE, Monterey, California, USA **2015**, p.1.
[19] M. Wang, J. Zhou, Y. Yang, S. Gaba, M. Liu, W. D. Lu, *Nanoscale* **2015**, *7*, 4964.
[20] J. Woo, W. Lee, S. Park, S. Kim, D. Lee, G. Choi, E. Cha, J. Lee, W. Jung, C. Park, H. Hwang, *VLSI* **2013**, p. T168.
[21] K. K. Likharev, *Appl. Phys. Lett.* **1998**, *73*, 2137.
[22] J. D. Casperson, L. D. Bell, H. A. Atwater, *J. Appl. Phys.* **2002**, *92*, 261.
[23] D. O. Scanlon, C. W. Dunnill, J. Buckeridge, S. A. Shevlin, A. J. Logsdail, S. M. Woodley, C. R. A. Catlow, M. J. Powell, R. G. Palgrave, I. P. Parkin, G. W. Watson, T. W. Keal, P. Sherwood, A. Walsh, A. A. Sokol, *Nat. Mater.* **2013**, *12*, 798.
[24] W.-S. Hwang, H.-C. Lee, *Mater. Trans. JIM* **2005**, *46*, 1942.
[25] V. Y. Q. Zhuo, Y. Jiang, M. H. Li, E. K. Chua, Z. Zhang, J. S. Pan, R. Zhao, L. P. Shi, T. C. Chong, J. Robertson, *Appl. Phys. Lett.* **2013**, *102*, 2011.
[26] J. Woo, J. Song, K. Moon, J. Lee, E. Cha, A. Prakash, D. Lee, S. Lee, J. Park, Y. Koo, C. Park, H. Hwang, *VLSI*, IEEE, Honolulu, Hawaii, USA **2014**, p.9
[27] L. Yu, C. Stampfl, D. Marshall, T. Eshrich, V. Narayanan, J. Rowell, N. Newman, A. Freeman, *Phys. Rev. B: Condens. Matter* **2002**, *65*, 245110.
[28] A. Chen, *IEEE Trans. Electron. Devices* **2013**, *60*, 1318.
[29] J. Zhou, K.-H. Kim, W. Lu, *IEEE Trans. Electron. Devices* **2014**, *61*, 1369.
[30] S. Somani, A. Mukhopadhyay, C. Musgrave, *J. Phys. Chem. C* **2011**, *115*, 11507.
[31] Z. Fang, H. C. Aspinall, R. Odedra, R. J. Potter, *J. Cryst. Growth* **2011**, *331*, 33.
[32] M. Ritala, P. Kalsi, D. Riihela, K. Kukli, *Chem. Mater.* **1999**, *11*, 1712.
[33] H. Kim, A. J. Kellock, S. M. Rossnagel, *J. Appl. Phys.* **2002**, *92*, 7080.
[34] T. J. Park, J. H. Kim, J. H. Jang, K. D. Na, C. S. Hwang, J. H. Kim, M. Kim, J. H. Choi, K. J. Choi, J. H. Jeong, T. J. Park, J. H. Kim, J. H. Jang, *Appl. Phys. Lett.* **2007**, *91*, 252106.
[35] C. M. Fang, E. Orhan, G. a. de Wijs, H. T. Hintzen, R. a. de Groot, R. Marchand, J.-Y. Saillard, G. de With, *J. Mater. Chem.* **2001**, *11*, 1248.
[36] C. R. Crowell, *Solid-State Electron.* **1969**, *12*, 135.
[37] C. Kittel, *Introduction to Solid State Physics*, Wiley, New York, **2005**.
[38] W. Jeon, S. H. Rha, W. Lee, Y. W. Yoo, C. H. An, K. H. Jung, S. K. Kim, C. S. Hwang, *ACS Appl. Mater. Inter.* **2014**, *6*, 7910.
[39] A. Paskaleva, D. Spassov, E. Atanassova, *J. Phys. D: Appl. Phys.* **2007**, *40*, 6709.
[40] V. A. Shvets, V. S. Aliev, D. V. Gritsenko, S. S. Shaimeev, E. V. Fedosenko, S. V. Rykhlitski, V. V. Atuchin, V. A. Gritsenko, V. M. Tapilin, H. Wong, *J. Non-Cryst. Solids* **2008**, *354*, 3025.
[41] W. Chun, A. Ishikawa, H. Fujisawa, T. Takata, J. N. Kondo, M. Hara, M. Kawai, Y. Matsumoto, K. Domen, *J. Phys. Chem. B* **2003**, *107*, 1798.